Graphene layer growth: Collision of migrating five-member rings

Russell Whitesides[a], Alexander C. Kollias[b,c], Dominik Domin[b], William A. Lester, Jr.[b,c], Michael Frenklach[a]

[a] *Department of Mechanical Engineering, University of California, Berkeley, CA 94720-1740 and Environmental Energy Technologies Division, Lawrence Berkeley National Laboratory, Berkeley, CA 94720, USA*

[b] *Kenneth S. Pitzer Center for Theoretical Chemistry, Department of Chemistry, University of California, Berkeley, CA 94720-1460*

[c] *Chemical Sciences Division, Lawrence Berkeley National Laboratory, Berkeley, CA 94720*

Corresponding author: Professor Michael Frenklach
Department of Mechanical Engineering
University of California at Berkeley
Berkeley, CA 94720-1740, USA
Phone: (510) 643-1676
Fax: (510) 643-5599
E-mail: myf@me.berkeley.edu

W O R D C O U N T

(Determined by Method 1)

Text (counted by MS Word 2003)	3227
40 References (40+2)*2.3*7.6	735
3 Equations (4+4+4)*7.6	92
5 Figures (435+386+122+175+250)	1368
4 Tables 4*((10+2)*7.6)	365
Abstract (not included in Total)	144
Total	5787

Accepted for Oral Presentation and Publication at

31st International Symposium on Combustion

University of Heidelberg, Germany, August 6-11, 2006

Abstract

A reaction pathway is explored in which two cyclopenta groups combine on the zigzag edge of a graphene layer. The process is initiated by H addition to a five-membered ring, followed by opening of that ring and the formation of a six-membered ring adjacent to another five-membered ring. The elementary steps of the migration pathway are analyzed using density functional theory to examine the region of the potential energy surface associated with the pathway. The calculations are performed on a substrate modeled by the zigzag edge of tetracene. Based on the obtained energetics, the dynamics of the system are analyzed by solving the energy transfer master equations. The results indicate energetic and reaction-rate similarity between the cyclopenta combination and migration reactions. Also examined in the present study are desorption rates of migrating cyclopenta rings which are found to be comparable to cyclopenta ring migration.

Keywords: Soot, PAH, Surface growth, Reaction mechanisms, HACA

1. Introduction

Soot formation is a persistent problem in fossil fuel combustion. About 80% of soot mass from combustion sources is estimated to originate from surface growth [1]. Recent modeling and interpretation of soot surface growth (e.g., [2-9]) has been done mostly by assumption of chemical similarity to reactions of gaseous aromatic species [10,11] and, specifically, by invoking the HACA mechanism [11-13]. This surface growth model is a repetitive reaction sequence of edge surface activation by gaseous hydrogen followed by addition of a gaseous hydrocarbon precursor (acetylene) to the surface radical site formed [12].

The initial surface HACA model was based on the armchair edges of aromatics [13], yet more recent work [14-18] has explored growth on zigzag edges, which can be formed by the filling of armchair edge boat sites. A gaseous acetylene molecule can adsorb onto an H-activated zigzag edge (i.e., add to a surface radical formed by H abstraction) and then react to form a five-membered, cyclopenta edge ring. Theoretical investigation of zigzag edge reactions identified the possibility of migration of cyclopenta rings along the zigzag edge,

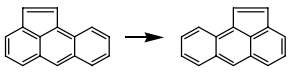

(1)

The overall step (1) consists of a series of unimolecular transformations of the chemisorbed C_2H_2 surface moiety mediated by hydrogen atoms [15,17].

The previous study [17] undertook a detailed analysis of the migration reaction: energetics were examined at several levels of quantum-chemical theory (DFT, MP2, and PM3), the elementary reaction rates of the migration process were obtained by solving energy transfer master equations (with the MultiWell code [19,20]), and graphene edge growth rates and evolving surface morphologies were obtained in sterically-resolved kinetic Monte Carlo (KMC) simulations by augmenting the migration kinetics with estimated rates for eight additional

surface steps describing adsorption, desorption, and transformation of the cyclopenta rings. The results obtained indicate that the migration step is sufficiently fast to compete effectively with other surface processes and thus should determine the resulting surface morphology and overall rate of surface growth. It is pertinent to mention that the kinetic model with the migration step included was shown to match closely experimental measurements of surface growth rates.

As one of the consequences of rapid surface migration, the previous authors [17] suggested that two migrating cyclopenta rings could react with one another to form a relatively stable surface species such as

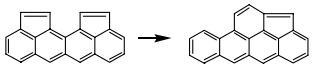 , (2)

possibly leading to graphene layer curvature. The latter phenomenon has mechanistic implications for the evolution of soot particle surface morphology, which has been receiving increasing attention [21-24], as well as to growth of fullerenic materials and carbon nanotubes [25,26].

The present study investigates this possibility, namely, the existence of an elementary-reaction pathway of combination of "colliding" cyclopenta rings on an aromatic zigzag edge. We report the potential-energy surface (PES) for the new pathway obtained with quantum-chemical calculations and reaction rates computed on the basis of these energetics. We compare computed reaction rates of the cyclopenta ring "collision" with rates of migration, as migration was one of the dominant steps of the previous kinetic model [17]. We also examine the contribution of desorption of reaction intermediates along the migration pathway.

2. Computational methods

2.1. Energetics

Density functional theory (DFT) was used to calculate the molecular and energetic parameters of all stable species and transition states involved in the cyclopenta migration and combination reaction sequences. The substrates for the two sets of calculations were modeled by the zigzag edges of anthracene and tetracene, respectively. These are the smallest aromatic molecules of sufficient size to represent the surfaces of interest, thereby minimizing computational expense.

Geometry optimizations were performed with the B3LYP hybrid functional [27] and the 6-311G(d,p) basis set. This level of theory is the highest deemed practical for the size of molecules in question. Previous studies have shown energetic predictions of B3LYP calculations at the 6-311G(d,p) level to be in good agreement with experimental and high-level ab initio results for stable species [16,28,29]. The energies of transition states predicted by this method, however, are often underestimated by about 5 kcal mol^{-1} [30,31]. This shortcoming lessens the accuracy of rate constants derived from the calculated energetics yet allows for an order-of-magnitude analysis.

Force calculations were performed at each predicted stationary point to confirm the point to be an energetic minimum (no imaginary frequencies) or a saddle point (one imaginary frequency). Transition states were confirmed to connect the reactant and product stable species by visual inspection of normal modes corresponding to the imaginary frequencies calculated at the B3LYP/6-311G(d,p) level and by intrinsic reaction coordinate calculations at the B3LYP/3-21G level. Zero point energies were determined from the force calculations and scaled by a

factor of 0.9668 [32]. All calculations were performed using the Gaussian 03 suite of codes [33] on an Intel Xeon cluster.

2.2. Kinetics

The kinetics of the reaction pathways were examined using the latest release of the MultiWell suite of codes [19,34]. MultiWell employs a stochastic approach to solution of the master equations for energy transfer in unimolecular reaction systems [19,35]. We performed computations for two models: thermal decomposition of radical intermediates, and chemically-activated combination of substrate molecules with gaseous H. Microcanonical rate constants for the elementary reactions of these models were calculated with MultiWell at the RRKM level of theory.

The key inputs to MultiWell—reaction barriers, frequencies, and moments of inertia—were assigned from the DFT calculations at the B3LYP/6-311G(d,p) level of the present study except where noted. Following Gilbert and Smith [36] the real frequencies below 150 cm^{-1} were examined by graphically visualizing the associated normal mode vibrations to identify internal rotational modes. Three modes were identified to have rotational character for stable species with an adsorbed $–C_2H_x$ group: a one-dimensional torsion of the adsorbate with respect to the substrate about the C_s–C bond and a two-dimensional precession rotation of the adsorbate. Potential energy barriers to torsional rotation were calculated by relaxed potential energy scans at the B3LYP/3-21G level and were on the order of 1-5 kcal mol^{-1}. Reduced moments of inertia (I_1) for the one-dimensional rotation were taken as calculated by the MultiWell routine MomInert [34]. The moment of inertia (I_2) for the precession rotation is a function of the precession angle and orientation of the one-dimensional rotor and can either be greater than or less than I_1. Since the precession angle was small, 1 to 5 degrees, I_2 was taken to be equal to I_1.

While the one-dimensional and two-dimensional rotations are probably coupled, the present calculations were conducted under the assumption that the two rotors are independent of each other. The sensitivity of the kinetics calculations to this assumption is discussed in Section 3.2.

The sums and densities of states for intermediate species and transition states were determined by exact count with a grain size of 10 cm^{-1}, maximum energy of 200,000 cm^{-1}, and the dividing level between the high and low energy regimes set at 2500 cm^{-1}. Suggested numerical tests [19,20] established that these settings provide sufficient accuracy for simulations of the systems being studied. Lennard-Jones parameters for the reactants and intermediates were taken from an empirical correlation [37]. Argon was chosen as the bath gas collider. The collisional energy transfer was treated by the exponential-down model with $\langle \Delta E_{down} \rangle = 260$ cm^{-1} based on the data of Hippler et al. [38].

MultiWell simulations were performed for temperatures ranging from 1500 to 2500 K and pressures ranging from 0.1 to 10 atm, spanning conditions from typical laboratory studies to practical combustion devices. The numerical runs were carried out for reaction times ranging from 1×10^{-7} to 6×10^{-5} s. For each set of conditions, between 1×10^{6} and 2.5×10^{7} stochastic trials were performed to maintain statistical error in the species fractions to within 1 to 4%.

3. Results and discussion

3.1. Simultaneous migration and desorption of cyclopenta rings

In the previous study [17], the rates of surface reactions other than the migration sequence were estimated based on chemical analogy. Specifically, the desorption rate of an adsorbed cyclopenta ring, reaction S2 in Ref. [17],

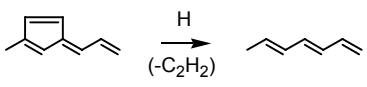

, (3)

was assumed to be initiated by H abstraction, independent of the cyclopenta ring migration step, which is initiated by H addition. Here we test this assumption by adding products of decomposition of the intermediate species to the cyclopenta migration reaction sequence. The relatively small size of the migration reaction system makes it computationally feasible to investigate the intrinsic competition between migration and desorption at the level of theory adopted in the present study.

The potential energy diagram for the augmented migration reaction sequence is shown in Fig. 1. The two additional desorption products are those numbered **6** and **7** and represent desorption of hydrogen atom and acetylene molecule, respectively. The transition state connecting species **6** and **4** was not found at the B3LYP/6-311G(d,p) level, yet a lower level calculation, at B3LYP/3-21G, resulted in a barrier below 0.1 kcal mol^{-1}. Thus, geometries and frequencies for the **6-4** transition state were taken from the B3LYP/3-21G calculations, and a barrier of 0.5 kcal mol^{-1} was assigned by analogy to that of reaction **1** $\rightarrow$ **2** obtained at the B3LYP/6-311G(d,p) level. The barriers leading to the two desorption products, **6** and **7**, are significantly higher than those of the steps producing the migration product, **1'**. For instance, when considering the chemically-activated combination of hydrogen atom with substrate species **1**, a 5 kcal mol^{-1} barrier must be overcome to form **1'**, while the barrier to formation of species **6** is 27 kcal mol^{-1} and that to **7** is 35 kcal mol^{-1}.

The reaction rate constants for production of **1'**, **6**, and **7** by thermal decomposition of **2** and by chemically-activated combination of H-atom with substrate molecule **1** are given in Tables 1-4. For comparison, the reaction rates for production of **1'** calculated excluding desorption product channels are given in the same tables. Inspection of the results indicates that cyclopenta ring desorption (**2** $\rightarrow$ **6** and **2** $\rightarrow$ **7** in Tables 1-3 and **1** $\rightarrow$ **6** and **1** $\rightarrow$ **7** in Table 4) approaches

and overcomes migration (**2** → **1** in Tables 1-3 and **1** → **1'** in Table 4) in the temperature range studied. As a consequence, the rate of migration decreases with the inclusion of desorption steps.

The results obtained demonstrate that the unimolecular decomposition of surface intermediates, including desorption of cyclopenta rings, is competitive with migration kinetics. Yet, the computed rates of these decomposition processes, reaction steps **2** → **6** and **2** → **7** in Tables 1-3, are on the order of 10^5 s^{-1} at high temperatures (or similarly steps **1** → **6** and **1** → **7** in Table 4) and hence are comparable with and even lower than those of bimolecular reactions of the decomposition products with gaseous species. For instance, at flame conditions, the rates of H addition to surface radicals or unsaturated C–C bonds are on the order of 10^6 s^{-1}. Such processes can contribute to deactivation of surface radicals and desorption of $–C_2H_x$ groups and, on the other hand, facilitate the return of these adsorbates to the cyclopenta form and thus enhance surface migration. A complete analysis calls for detailed kinetic Monte Carlo (KMC) simulations with inclusion of all possible reactions of surface intermediates with gaseous species and individual treatment of intermediates. In addition to a substantially increased computational burden of such level of calculations [39], they require establishing further details of the underlying kinetic mechanism. The complexity of the zigzag edge reaction network is clearly demonstrated by the new reaction, combination of migrating cyclopenta rings, discussed in Section 3.3.

3.2. Internal rotations

Visual inspection of the normal modes indicates that precession rotation is present in species **3**, **4**, and **5** and that species **3** and **5** also exhibit one-dimensional rotation. The C_s–C bond in species **4**, similar to the recently discussed C_6H_5–CCH_2 bond [40], has strong double bond

character that produces high barriers to torsional motion, and hence this motion was modeled as a harmonic oscillator. Sensitivity of the computed rate constants to the treatment of internal rotations in species **3**, **4**, and **5** was examined by considering five test cases: case A was as described in Section 2.2 with I_2 equal to I_1; case B was the same as case A except that barriers to rotation were set to zero; case C set I_2 to half I_1; case D set I_2 to twice I_1; and case E treated the precession modes by the harmonic oscillator approximation.

The 1 atm overall migration reaction rate constants computed for all test cases deviate from each other by less than 4%. This result may seem surprising considering the difference one sees in microcanonical rate constants for such varied treatment of internal rotations. However, the low sensitivity can be explained by the fact that the rate limiting step of this reaction system is β-scission, reaction step **2** $\rightarrow$ **3**, which is not affected by the treatment of internal rotation. Even the extreme case of treating the precession rotation by the harmonic oscillator model does not significantly affect the resultant rate constants. We conclude that the overall rate constants are not significantly affected by the details of the treatment of internal rotations, and on the basis of this conclusion the remainder of the MultiWell calculations was performed with I_2 set to I_1 and free rotation of one-dimensional internal rotors.

3.3. Combination of cyclopenta rings

A mechanism was constructed for the combination of cyclopenta groups, reaction (2), by exploring the PES connecting the product and reactant of this reaction to identify and characterize intermediate stable species and transition states. The computed B3LYP/6-311G(d,p) PES is shown in Fig. 2. The transition state connecting species **9** and **8** was not found at the B3LYP/6-311G(d,p) level. Similar to the **6-4** transition state discussed in Section 3.1, geometries and frequencies for the **9-8** transition state were taken from calculations at the

B3LYP/3-21G level and a barrier of 0.5 kcal mol^{-1} was assumed. Inspection of the PES in Fig. 2 shows topography similar to that of the migration pathway shown in Fig. 1. When considering the chemically-activated combination of H with substrate molecule **8**, the largest barrier along the dominant path from species **8** to **16** is 8 kcal mol^{-1}. The analogous barrier height in the migration path is 5 kcal mol^{-1}.

Torsional motion of the $-C_2H_x$ group was identified in species **10**, **11**, and **13** and was treated as a one-dimensional free rotation. Similar to the treatment of species **4** discussed earlier, the torsional motion of the adsorbate of species **12** was modeled as a harmonic oscillator. Species **10**, **11**, **12**, and **13** were found to exhibit precession rotation.

We had anticipated that the graphene edge molecular complex composed of adjacent five- and six-membered rings would result in strained geometry, leading to graphene sheet curvature thereby relieving the strain. This expectation was partially confirmed—the B3LYP/6-311G(d,p) geometry of product species **16** (Fig. 3) does show deformation of the surface and substrate rings. However, this deformation does not produce sheet curvature but largely in-plane distortion of rings adjacent to the cyclopenta ring (such as six-membered rings 9-14 and 15-21 in Fig. 3). Such ring distortion exists in all the species to some extent but is most pronounced in species **16**. As a measure of the relative deformation, the angle formed by substrate carbon atoms labeled 7, 9, and 11 in Fig. 3 is calculated to be 8.9º for species **16** and 6.2º for species **8**. It is possible that still larger graphene sheets may experience bending due to a more constrained environment of cyclopenta rings, a subject of future research as calculations of such larger molecular substrate models become computationally feasible at a reliable level of quantum theory.

The reaction rates for production of **16** by thermal decomposition of **9** and by chemically activated combination of H-atom with substrate species **8** are shown in Tables 1-4. The chemical activation rate constants showed no substantial pressure dependence indicating that the high pressure limit for these reactions has been reached and hence the derived rates are applicable to reactions occurring on larger substrates, consistent with previous results [17]. However, at lower pressures and temperatures considered here, time-dependent solution of master equations revealed that the reaction systems do not attain a steady state on a time of scale of 1 μs, as illustrated in Fig. 4. The relatively large relaxation times indicate that the surface sites may not be completely deactivated at the time of their collisions with gaseous species, the latter occurring possibly on a time scale of 0.1–1 μs at flame conditions, thus affecting surface reaction kinetics.

Inspection of the results reported in Tables 1-4 indicates that the computed cyclopenta combination reaction rates are of the same order of magnitude as those of cyclopenta migration. This result should not be surprising in light of the energetic similarity of the two pathways. The near equality of cyclopenta combination and migration rates indicates that, for conditions at which the migration reaction dominates, migration of multiple rings will lead to a significant number of cyclopenta collision events. Furthemore, the product of the cyclopenta combination reaction, species **16**, is relatively thermodynamically stable—the equilibrium constant of **8** = **16** is computed to be 16.5 at 1500 K and 5.1 at 2500 K.

The previous work [17] concluded that migration of five-membered rings along the edge and formation of six-membered rings at the corners of the zigzag edge were the key mechanistic features determining surface growth rates and morphology. Without cyclopenta collisions, the layer buildup originates at the corners of a zigzag edge and spreads across the edge as migrating cyclopenta rings transform into six member rings upon reaching the six-membered-ring corner,

as illustrated in the left panel of Fig 5. Combination of cyclopenta groups (as well as possible combination of gaseous acetylene with a cyclopenta group, proceeding via **11** $\rightarrow$ **16**) allows layer building to originate in the center and propagate outwards, as shown in the right panel of Fig. 5. This "inside-out" layer building mechanism will result in incorporation of five-membered rings into the graphene sheet, which in turn can lead to sheet curvature or formation of surface inactive sites at the next layer. The next question to answer, though, is the kinetic stability of the cyclopenta combination product, species **16**: will it rapidly add another six-membered ring, thus "forcing" sheet curvature and continuation of graphene edge growth, or will it decompose back to migrating cyclopenta rings? These and related reaction pathways will be a subject of our future investigation.

5. Conclusions

The present results identify two new mechanistic features of aromatic-edge growth: (1) combination of (migrating) cyclopenta rings forms a relatively thermodynamically stable species that can serve as a middle-edge nucleating site, and (2) desorption of migrating cyclopenta rings is intrinsically coupled to the migration reaction pathway. Both of these new processes are comparable in rate to cyclopenta migration, which calls for establishing these mechanisms in fuller detail. The latter knowledge will bring us closer to detailed kinetic Monte Carlo simulations of graphene edge buildup, the rate of appearance of surface defects, and the amount of surface curvature.

Acknowledgments

Russell Whitesides, Alexander C. Kollias, William A. Lester, Jr., and Michael Frenklach were supported by the Director, Office of Energy Research, Office of Basic Energy Sciences, Chemical Sciences, Geosciences and Biosciences Division of the US Department of Energy,

under Contract No. DE-AC03-76F00098. Dominik Domin was supported by the CREST Program of the National Science Foundation under Grant No. HRD-0318519.

References

[1] B.S. Haynes, H.G. Wagner, *Z. Phys. Chem. N. F.* 133 (1982) 201-213.

[2] J. Appel, H. Bockhorn, M. Frenklach, *Combust. Flame* 121 (2000) 122-136.

[3] F. Xu, G.M. Faeth, *Combust. Flame* 125 (2001) 804-819.

[4] M. Balthasar, F. Mauss, A. Knobel, M. Kraft, *Combust. Flame* 128 (2002) 395-409.

[5] B. Zhao, Z. Yang, M.V. Johnson, H. Wang, A.S. Wexler, M. Balthasar, M. Kraft, *Combust. Flame* 133 (2003) 173-188.

[6] A. Violi, *Combust. Flame* 139 (2004) 279-287.

[7] M.S. Skjøth-Rasmussen, P. Glarborg, M. Østberg, J.T. Jahannessen, H. Livbjerg, A.D. Jensen, T.S. Christensen, *Combust. Flame* 136 (2004) 91-128.

[8] L. Wang, D.C. Haworth, S.R. Turns, M.F. Modest, *Combust. Flame* 141 (2005) 170-179.

[9] J.Z. Wen, M.J. Thomson, S.H. Park, S.N. Rogak, M.F. Lightstone, *Proc. Combust. Inst.* 30 (2005) 1477-1484.

[10] M. Frenklach, in: J.C. Tarter, S. Chang, D.J. DeFrees (Eds.), *Carbon in the Galaxy: Studies From Earth and Space*. NASA Conference Publication 3061, 1990, pp. 259-273.

[11] M. Frenklach, D.W. Clary, W.C. Gardiner, Jr., S.E. Stein, *Proc. Combust. Inst.* 20 (1985) 887-901.

[12] M. Frenklach, *Phys. Chem. Chem. Phys.* 4 (2002) 2028-2037.

[13] M. Frenklach, H. Wang, *Proc. Combust. Inst.* 23 (1991) 1559-1566.

[14] M. Frenklach, *Proc. Combust. Inst.* 26 (1996) 2285-2293.

[15] M. Frenklach, N.W. Moriarty, N.J. Brown, *Proc. Combust. Inst.* 27 (1998) 1655-1661.

[16] N.W. Moriarty, N.J. Brown, M. Frenklach, *J. Phys. Chem. A* 103 (1999) 7127-7135.

[17] M. Frenklach, C.A. Schuetz, J. Ping, *Proc. Combust. Inst.* 30 (2005) 1389-1396.

[18] N.D. Marsh, M.J. Wornat, *Proc. Combust. Inst.* 28 (2000) 2585-2592.

[19] J.R. Barker, *Int. J. Chem. Kinet.* 33 (2001) 232-245.

[20] J.R. Barker, N.F. Ortiz, *Int. J. Chem. Kinet.* 33 (2001) 246-261.

[21] R.H. Hurt, G.P. Crawford, H.S. Shim, *Proc. Combust. Inst.* 28 (2000) 2539-2546.

[22] A.B. Palotás, L.C. Rainey, C.J. Feldermann, A.F. Sarofim, J.B.V. Sande, *Microscopy Res. Tech.* 33 (1996) 266-278.

[23] A.C. Barone, A. D'Alessio, A. D'Anna, *Combust. Flame* 132 (2003) 181-187.

[24] A. Braun, N. Shah, F.E. Huggins, K.E. Kelly, A.F. Sarofim, C. Jacobsen, S. Wirick, H. Francis, J. Ilavsky, G.E. Thomas, G.P. Huffman, *Carbon* 43 (2005) 2588-2599.

[25] L.R. Radovic, B. Bockrath, *J. Am. Chem. Soc.* 127 (2005) 5917-5927.

[26] G.L. Dong, K.J. Huttinger, *Carbon* 40 (2002) 2515-2528.

[27] A.D. Becke, *J. Chem. Phys.* 98 (1993) 5648-5652.

[28] M.R. Nimlos, J. Filley, J.T. McKinnon, *J. Phys. Chem. A* 109 (2005) 9896-9903.

[29] J. Cioslowski, P. Piskorz, D. Moncrieff, *J. Am. Chem. Soc.* 120 (1998) 1695-1700.

[30] J.P.A. Heuts, R.G. Gilbert, L. Radom, *J. Phys. Chem.* 100 (1996) 18997-19006.

[31] J.L. Durant, *Chem. Phys. Lett.* 256 (1996) 595-602.

[32] R.D. Johnson, III (Ed.) *NIST Computational Chemistry Comparison and Benchmark Database*. National Institute of Standards and Technology, Aug 2005; http://srdata.nist.gov/cccbdb.

[33] M.J. Frisch, *et al.*, Gaussian 03, Revision C.02, Gaussian, Inc., Wallingford, CT, 2004;

[34] J.R. Barker, N.F. Ortiz, J.M. Preses, L.L. Lohr, MultiWell, 1.4.1, 2004; http://aoss.engin.umich.edu/multiwell/.

[35] J.R. Barker, L.M. Yoder, K.D. King, *J. Phys. Chem. A* 105 (2001) 796-809.

[36] R.G. Gilbert, S.C. Smith, *Theory of Unimolecular and Recombination Reactions*. Blackwell-Scientific, Oxford, 1990.

[37] H. Wang, M. Frenklach, *Combust. Flame* 96 (1994) 163-170.

[38] H. Hippler, J. Troe, H.J. Wendelken, *J. Chem. Phys.* 78 (1983) 6709-6717.

[39] A. Netto, M. Frenklach, *Diamond Relat. Mater.* 14 (2005) 1630-1646.

[40] I.V. Tokmakov, M.C. Lin, *J. Am. Chem. Soc.* 125 (2003) 11397-11408.

Table 1
Thermal decomposition rate constants, in s^{-1}, at 1 atm

Reaction	Temperature (K)		
	1500	2000	2500
2 → **1'** [a]	1.6×10^{4}	9.5×10^{4}	2.0×10^{5}
2 → **1'**	1.6×10^{4}	6.7×10^{4}	5.9×10^{4}
2 → **6**	8.9×10^{2}	4.6×10^{4}	2.4×10^{5}
2 → **7**	9.6×10^{1}	8.6×10^{3}	5.1×10^{4}
9 → **16**	1.3×10^{4}	1.5×10^{5}	4.9×10^{5}

(a) Without desorption product channels

Table 2
Thermal decomposition rate constants, in s^{-1} at 0.1 atm

Reaction	Temperature (K)		
	1500	2000	2500
2 → **1'** [a]	3.5×10^{3}	1.5×10^{4}	3.2×10^{4}
2 → **1'**	3.4×10^{3}	1.1×10^{4}	8.3×10^{3}
2 → **6**	9.8×10^{1}	7.2×10^{3}	3.4×10^{4}
2 → **7**	1.0×10^{1}	1.3×10^{3}	7.1×10^{3}
9 → **16**	3.2×10^{3}	2.7×10^{4}	7.5×10^{4}

(a) Without desorption product channels

Table 3
Thermal decomposition rate constants, in s^{-1} at 10 atm

Reaction	Temperature (K)		
	1500	2000	2500
2 → **1'** [a]	5.7×10^{4}	5.3×10^{5}	1.3×10^{6}
2 → **1'**	5.3×10^{4}	3.6×10^{5}	3.6×10^{5}
2 → **6**	7.4×10^{3}	2.8×10^{5}	1.5×10^{6}
2 → **7**	9.8×10^{2}	4.9×10^{4}	3.2×10^{5}
9 → **16**	3.0×10^{4}	7.2×10^{5}	2.8×10^{6}

(a) Without desorption product channels

Table 4
Chemical activation rate constants, in $cm^3mol^{-1}s^{-1}$ at 1 atm

Reaction	Temperature (K)		
	1500	2000	2500
1 → **1'** [a]	5.6×10^{11}	1.0×10^{12}	1.6×10^{12}
1 → **1'**	4.6×10^{11}	3.6×10^{11}	1.9×10^{11}
1 → **6**	1.7×10^{11}	1.1×10^{12}	2.3×10^{12}
1 → **7**	2.7×10^{10}	2.2×10^{11}	4.6×10^{11}
8 → **16**	1.5×10^{12}	3.5×10^{12}	6.0×10^{12}

(a) Without desorption product channels

Figure Captions

Figure 1. Potential energy diagram of the migration pathway including desorption species.

Figure 2. Potential energy diagram of the cyclopenta combination reaction pathway.

Figure 3. Equilibrium geometry of cyclopenta combination product, species **16**.

Figure 4. Time dependant species fractions for chemically-activated combination of H with substrate species **8** at 1500 K and 1 atm.

Figure 5. Layer building initiated by corner-nucleated six-membered rings (left) and by combination of edge cyclopenta groups (right).

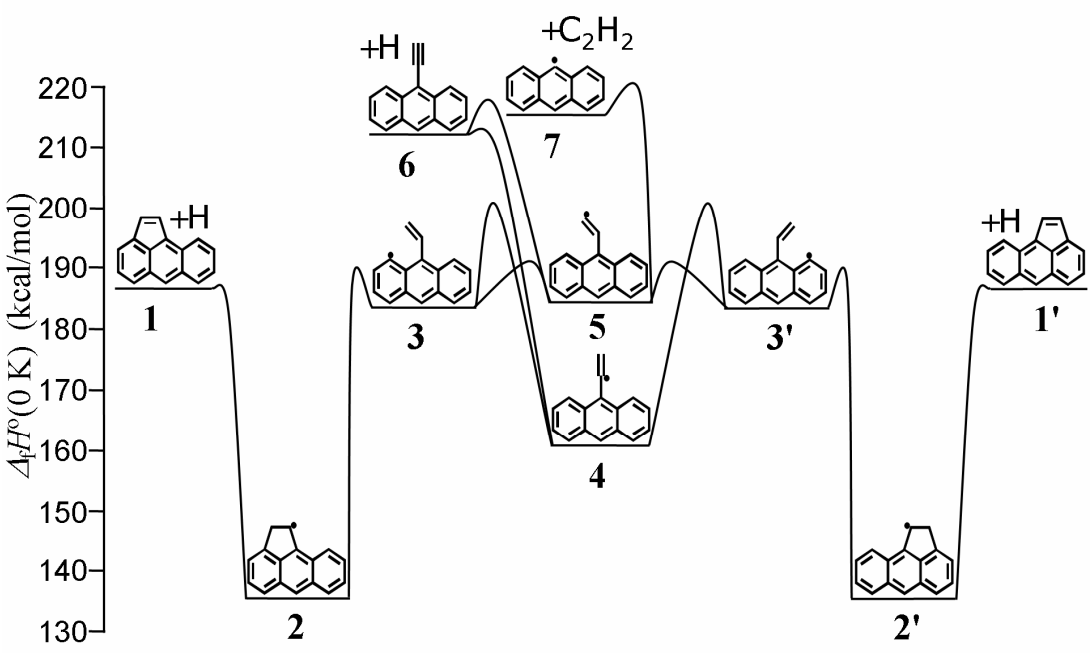

Fig. 1. Potential energy diagram of the migration pathway including desorption species.
(Two Column/ Height = 86.6 mm = 425 words + caption = 435)

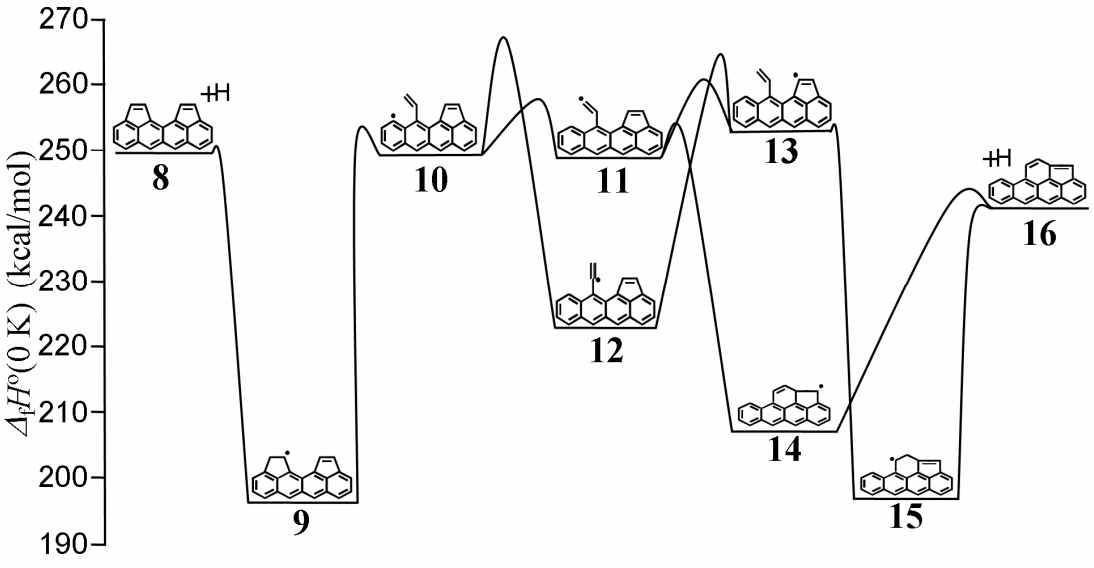

Fig. 2. Potential energy diagram of the cyclopenta combination reaction pathway.
(Two Column/ Height = 75.7 mm = 377 words + caption = 386)

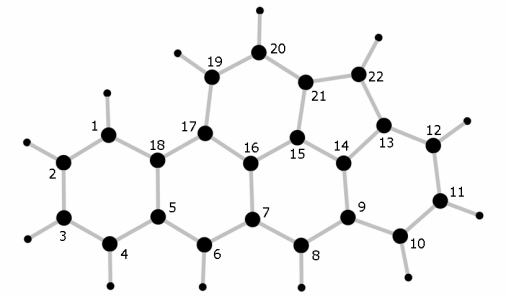

Fig. 3. Equilibrium geometry of cyclopenta combination product, species **16**.
(One column/ Height = 41.4 mm = 114 words + caption = 122)

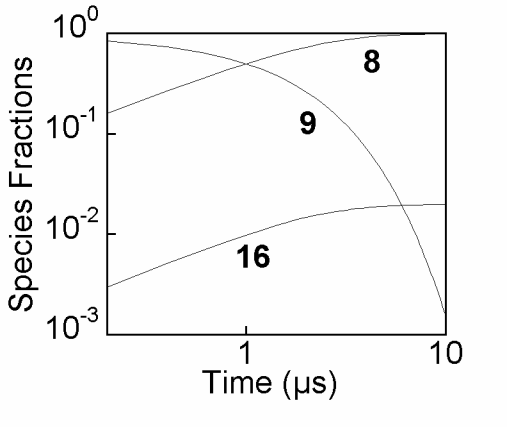

Fig. 4. Time dependant species fractions for chemically-activated combination of H with substrate species **8** at 1500 K and 1 atm.
(One column/Height = 61.5 mm = 156 words + caption = 175)

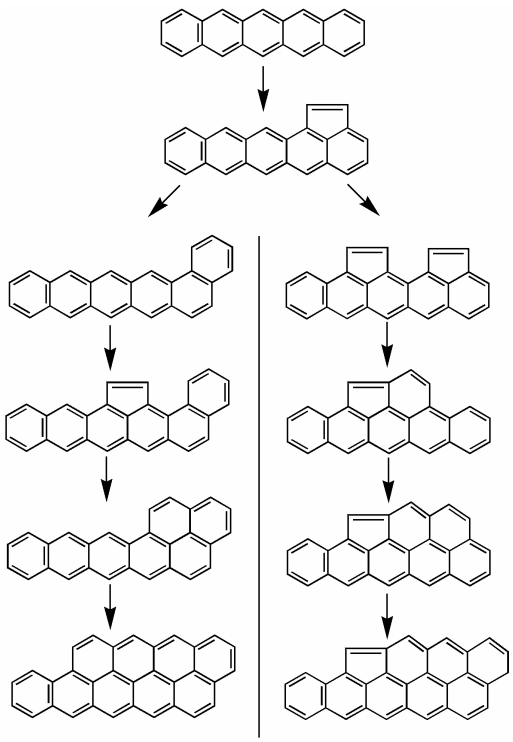

Fig. 5. Layer building initiated by corner-nucleated six-membered rings (left) and by combination of edge cyclopenta groups (right).
(One column/ Height = 96.5 mm = 234 words + caption = 250)